Journal of *Marine Science and Engineering*

MDPI

Review

Ferdinandea Island and Graham Bank, Sicily Channel: An Integrated Historical, Geological and Geomorphological Synthesis of a Shallow Submarine Monogenetic Volcanic Field

Daniele Spatola [1,*], Luca Basilone [2,*], Fabiano Gamberi [3], Francesco Latino Chiocci [1,4], Gualtiero Basilone [5] and Attilio Sulli [6]

[1] Department of Earth Sciences, Sapienza University of Rome, 00185 Rome, Italy; francesco.chiocci@uniroma1.it
[2] Instituto Oceanográfico da Universidade de São Paulo, São Paulo 05508-120, Brazil
[3] Institute of Marine Sciences (ISMAR), Consiglio Nazionale delle Ricerche (CNR), 40129 Bologna, Italy; fabiano.gamberi@cnr.it
[4] Institute of Environmental Geology and Geo-Engineering (IGAG), Consiglio Nazionale delle Ricerche (CNR), 00185 Rome, Italy
[5] Consiglio Nazionale delle Ricerche (CNR) di Capo Granitola, 91021 Campobello di Mazara del Vallo, Italy; gualtiero.basilone@cnr.it
[6] Department of Earth and Marine Sciences, University of Palermo, 90123 Palermo, Italy; attilio.sulli@unipa.it
* Correspondence: daniele.spatola@uniroma1.it (D.S.); luca.basilone03@gmail.com (L.B.)

Abstract

Ferdinandea Island, part of a shallow-water submarine volcanic field, emerged in the Sicily Channel between Italy and Tunisia in July 1831 and was eroded below sea level within months; its submerged remnant forms the shallowest water depth region of Graham Bank. Here, we review nearly two centuries of historical accounts, geological interpretations and geomorphological data analysis and reassess them against high-resolution multibeam bathymetry, sub-bottom profiles (CHIRP) and published multichannel seismic data. The field comprises six volcanic edifices (V1–V6), 100–170 m high, located along structural trends characteristic of the Sicily Channel Rift. V3, the shallowest edifice, is the remnant of Ferdinandea Island formed during the 1831 Surtseyan eruption. Its flat summit, wave-reworked terrace and steep flanks record rapid post-eruptive modification. Historical observations and hydrographic surveys document the destruction of the emergent island and a further ~6 m lowering of its shallowest point between 1883 and 2012–2015; the separate contributions of wave erosion, subsidence and gravitational adjustment cannot be resolved from the available data. The same regional structural framework appears to have governed the distribution of the other volcanic centres, pockmarks, erosional escarpments and mass-transport deposits of the study area. Seventeen pockmarks, up to ~540 m wide and 22 m deep, occur as isolated, clustered and locally aligned depressions; they are associated with subsurface concave-upward reflectors and local water-column acoustic anomalies, consistent with focused fluid escape. Failures of volcanic and sedimentary slopes are widespread, with the largest debris-avalanche deposit covering ~2.2 km^2. Taken together, these observations indicate that tectonics, volcanism, fluid migration, wave- and bottom-current reworking, and gravitational instability have operated over different timescales to shape Graham Bank. Ferdinandea thus offers a rare historical and geological reference for investigating the rapid construction, degradation and long-term evolution of shallow-water volcanic edifices and highlights the still-open questions regarding the evolution and fate of ephemeral volcanic islands.

Check for updates

Academic Editors: Manuel Martín-Martín and Chun-Feng Li

Received: 13 July 2026
Revised: 29 July 2026
Accepted: 6 August 2026
Published: 7 August 2026

Copyright: © 2026 by the authors. Licensee MDPI, Basel, Switzerland. This article is an open access article distributed under the terms and conditions of the Creative Commons Attribution (CC BY) license.

Keywords: Ferdinandea Island; Sicily Channel; multibeam bathymetry; seismic reflection; submarine volcanism; pockmarks; mass-transport deposits; marine geohazard

1. Introduction

The Sicily Channel, in the central Mediterranean, is characterised by active extensional tectonics, widespread submarine volcanism and complex interactions among tectonic, magmatic, fluid-flow, mass-wasting and sedimentary processes (Figure 1) [1–4]. Within this setting, Graham Bank is a natural laboratory for investigating the morphology, evolution and instability of shallow-water volcanic edifices (Figure 1). It hosts a volcanic field known for the 1831 eruption that produced the ephemeral Ferdinandea Island [5], among the most extensively documented historical submarine eruptions of the Mediterranean. Despite this historical prominence, the long-term geomorphological evolution of the edifice and the processes controlling seafloor instability remain poorly constrained.

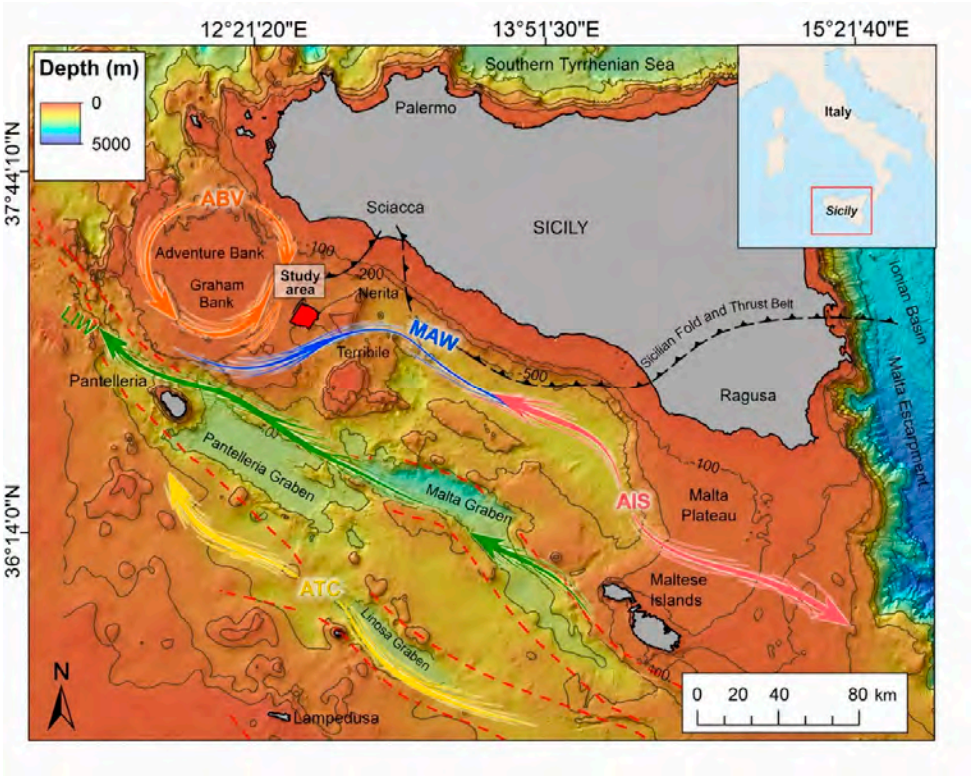

Figure 1. Bathymetric map of the Sicily Channel and adjacent areas showing the morphostructural setting and the location of the study area (red box, offshore Sciacca). Main isobaths (100, 200, 500 and 1000 m) are shown as contour lines, and the principal fault systems and grabens (Pantelleria, Malta, Linosa) are marked by red dashed lines. The inset shows the geographic location within Sicily. Levantine Intermediate Water (LIW), Modified Atlantic Water (MAW), Atlantic Tunisian Current (ATC), Atlantic Ionian Stream (AIS) and Adventure Bank Vortex (ABV). Bathymetric data from EMODnet Bathymetry (https://emodnet.ec.europa.eu/en/bathymetry; accessed on 9 July 2026).

Understanding of the geology of the site has advanced substantially through the recent application of high-resolution multibeam echosounding, sub-bottom CHIRP profiling, multichannel seismic reflection and ROV surveys [6–8]. However, previous studies have generally addressed the eruptive event, the volcanology of the field, or local seafloor mapping separately. An integrated synthesis combining historical observations, high-

resolution geomorphology, subsurface architecture and mass-wasting processes within a single evolutionary framework is still lacking.

Here, we review nearly two centuries of observations on Ferdinandea Island and Graham Bank, from the emergence of the island in 1831 to its present submerged state, and reassess them against high-resolution geophysical data. This review aims at establishing how volcanic, tectonic, fluid-flow, sedimentary and mass-wasting processes have acted together, and over different timescales, to shape the seafloor in the area of the volcanic field. Three objectives are addressed: (1) the framing of the emergence of Ferdinandea within the geological and tectonic setting of the Sicily Channel; (2) the assessment of the volcanic and post-eruptive processes responsible for the construction and subsequent submergence of the island; and (3) the analysis of the environmental and geohazard implications of the system.

2. Historical Context

In July 1831, a submarine eruption began in the waters southwest of Sicily. Fishermen reported discoloured water, floating pumice, gas emissions and anomalous wave patterns in the days preceding the emergence of an island above sea level [5,9]. According to the records compiled by Washington (1909) [10], the island grew rapidly to a reported height of approximately 60 to 200 m and a maximum area of 1 to 4 hectares. The speed of emergence allowed the organisation of contemporary expeditions within days, and the direct observation of an active volcanic process provided a rare opportunity for nineteenth-century geology [5,10].

The emergent island was built mainly of fragmental volcanic deposits, such as scoria, pumice and lithic material, rather than of consolidated lava flows [11,12]. This lithologic composition was critical to its successive evolution, because, once the edifice emerged, the poorly consolidated material was highly susceptible to wave erosion and subaerial degradation. The eruptive style was Surtseyan, that is, a submarine to subaerial explosive style with phreatomagmatic processes and products [13]. Pumice samples that floated across the Mediterranean were later collected and preserved at the Gemmellaro Museum of the University of Palermo [10]. They provide insights into the magmatic composition and mantle sources of the erupted material and of the Sicily Channel volcanism in general [14].

The name “Ferdinandea Island” reflects the political context of the time: the island was named after Ferdinand II, King of the Two Sicilies, since in 1831, the area in which it emerged was in waters pertaining to the Kingdom of the Two Sicilies. However, its appellation varied with the nationality of the observers [9,10]. In fact, British sailors from Malta were the first to arrive at the site of the island emergence and claimed it for the Crown as Graham Island. A French scientific expedition also landed and named it Île Julia (since it emerged in July). The competing claims prompted a short-lived diplomatic dispute, which became moot as the island was rapidly eroded. By early 1832, within months of its emergence, Ferdinandea had been reduced below sea level [5,6], leaving the submerged edifice today known as Graham Bank. The episode, retold in detail by Mazzarella (2013) [15], also left a mark on the history of geology: Charles Lyell used Graham Island in the craters-of-elevation controversy as first-hand evidence of how quickly a volcanic edifice can be built and destroyed [9].

Historical descriptions indicate that the island reached about 60 m above sea level during the eruptive phase, but had been reduced to about 20 m by late September 1831, to less than 1 m by late October, and was fully submerged between December 1831 and January 1832 [6,10]. Subsequent hydrographic surveys recorded the shallowest point at approximately 3 m below sea level in 1883, 8 m in 1914 and 9 m in 2012–2015 [6,8,16]. Because these values derive from different survey technologies and vertical-reference conventions,

the century-scale comparison is approximate. It documents about 6 m of additional lowering of the shallowest point since 1883, whereas the 25–28 m-deep summit terrace represents a broader wave-abraded surface rather than a direct measure of summit subsidence.

3. Regional Geological Setting

3.1. Sicily Channel Rift

The Sicily Channel occupies a key position at the boundary between the northward-moving African plate and the European plate, where regional convergence is accompanied by local extension within the Sicily Channel [17]. This interaction produced a complex extensional tectonic setting resulting in crustal stretching and thinning [2]. Structurally, the channel is dominated by NW–SE oriented, steeply dipping normal faults active since the Neogene and up to the Quaternary [1,17]. These faults belong to the Sicily Channel Rift Zone [18], a major expression of continental extension within the African to European plate boundary [1,19]. The Sicily Channel Rifting started in the Early Pliocene and significantly affected the continental crust. Crustal thickness decreases from approximately 30 km beneath the stable continental Sicily to 5 to 18 km in the rift zone [17]. This thinning, combined with the upward flow of hot mantle, favours melting and magma generation. The opening of three elongate depressions, namely the Pantelleria, Malta and Linosa grabens, reflects the regional extension [17,20]. The numerous submarine and subaerial volcanic edifices of the region demonstrate the link between lithospheric extension and magmatism, and the well-developed pattern of normal faults with associated seismicity confirms that tectonic activity persists to the present day [21].

The sedimentary succession of the Sicily Channel records a long history of sedimentation and volcanism in the Pelagian Platform. The general petrological characteristics of the Sicily Channel volcanism indicate an anorogenic magmatic affinity comparable to that of continental rift settings [14,20]. The uppermost units, composed of Plio-Pleistocene terrigenous, pelagic and hemipelagic sediments, reach thicknesses of up to 300 m and represent the most recent depositional sequences [22–24]. Beneath them lies a thicker and more complex succession that exceeds 4 km and spans the interval from the Triassic to the Miocene. This deeper succession comprises Miocene to Cretaceous shelf-edge carbonate build-ups and Cretaceous to Triassic shallow-platform carbonates [25,26]. The carbonate sequences are interrupted by extensive depositional hiatuses and are interbedded with tuffs and pillow lavas that record numerous volcanic episodes [27]. This alternation reflects the complex evolution of the Pelagian Platform, where submarine volcanism and carbonate sedimentation operated simultaneously over long timescales.

3.2. Volcanological Framework and Magmatic Characteristics

Volcanism in the Sicily Channel reflects the rift setting and the proximity of the African plate [14]. Radiometric dating constrains several temporal markers: the oldest documented magmatic products from the Nameless Bank are Late Miocene in age (9.5 ± 0.4 Ma) [28]; extensive Plio-Pleistocene submarine volcanism accompanied active rifting [28]; and historical volcanism, including activity during the First Punic War (264–241 BCE [29]), seventeenth to twentieth-century activity, and the 1831 emergence of Ferdinandea, confirms that the region is volcanically active [6,7].

The isotopic and petrological characteristics of the Graham Bank volcanic products constrain their magmatic sources. Volcanic rocks from the region indicate mantle-derived contributions [14], confirming the role of deep crustal and mantle processes in sustaining volcanism. Stable-isotope analysis of fluid inclusions points to multiple contributing sources, including magmatic volatiles, crustal fluids and potentially organic-derived com-

ponents [30]. This compositional and isotopic diversity reflects the complexity of magma generation and evolution in the continental rift.

4. Materials and Methods

The study area encompasses approximately 100 km^2 of seafloor at water depths ranging from 10 to 350 m (Figure 2). It is located along the western margin of a broader triangular morphological high (about 360 km^2) that extends south-eastward from the Adventure Bank and comprises the Graham (~10 m), Nerita (~16 m) and Terribile (~20 m) banks (Figure 1). Our analysis integrates three datasets: two acquired during the CNR ACUSCAL 2015 oceanographic cruise aboard the R/V Minerva-1, within the framework of the RITMARE Project (IAMC-CNR, Capo Granitola), and one previously published dataset [3].

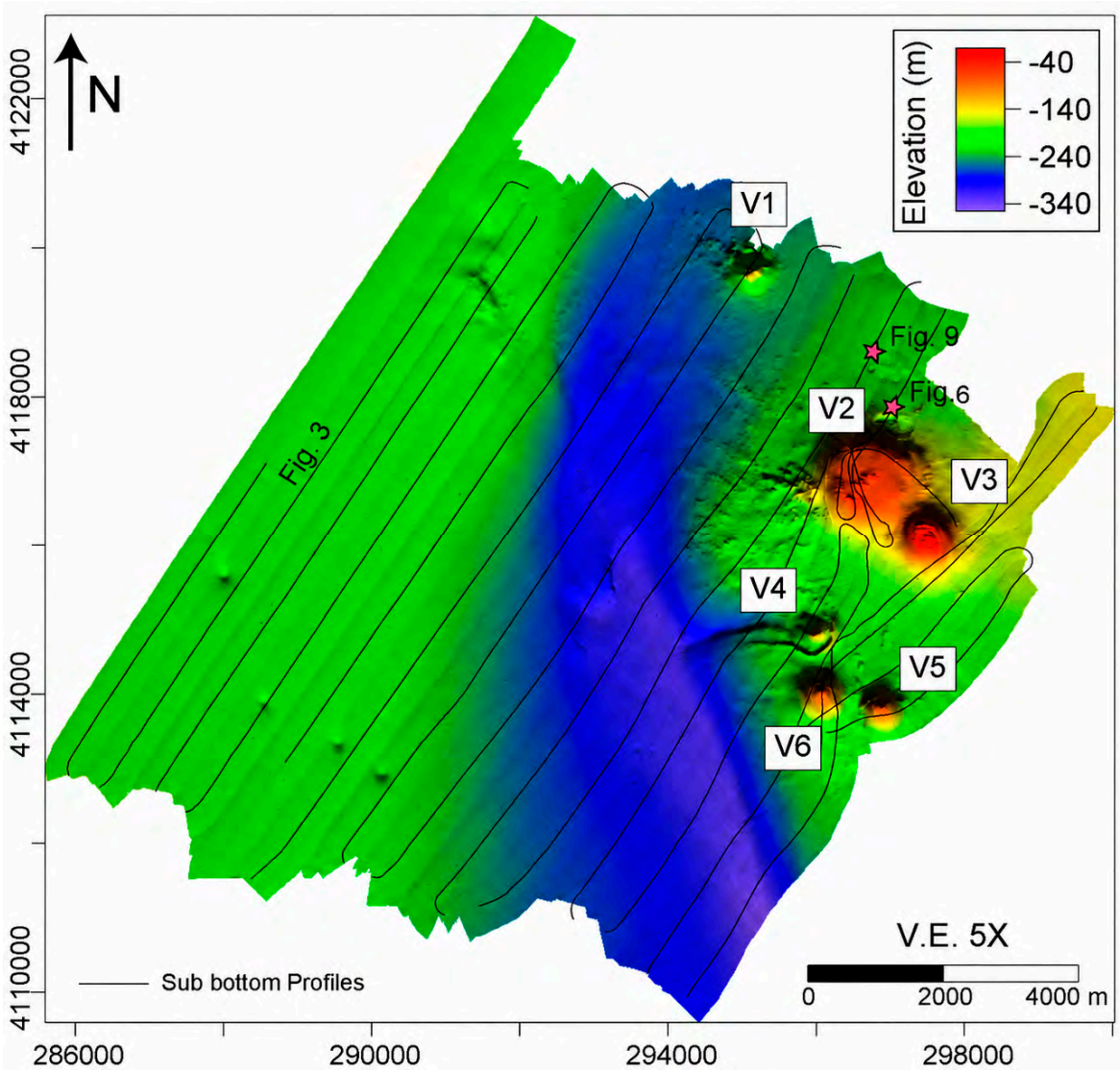

Figure 2. Shaded-relief bathymetric map of the study area showing data coverage. The colour scale indicates elevation (in metres); black lines mark the sub-bottom profiles. The six volcanic edifices (V1 to V6) are labelled. Coordinates in UTM Zone 33N (m); vertical exaggeration 5×. Starts indicate locations of Figures 6 and 9.

The first dataset consists of a high-resolution multibeam bathymetric survey performed with a Reson SeaBat 7160 echosounder (512 beams; nominal frequency of 44 kHz),

with positioning provided by a FUGRO SEASTAR differential GPS. The data were processed using PDS-2000 software, including erroneous-beam removal, noise filtering, calibration, navigation processing and sound-velocity correction. They have provided a digital terrain model with a final grid-cell size of 5 × 5 m, from which maps were generated in ArcMap 10.8. Residual noise, attributed to imperfect roll calibration and/or inaccuracies in the sound-velocity profile under adverse acquisition conditions, was minimised during post-processing. A formal total propagated uncertainty is not available for this legacy survey; inspection of residual striping indicates a local relative vertical uncertainty in the order of 0.5–1 m in the noisiest sectors. These artefacts may locally affect slope and relief estimates for the smallest features, but have a limited influence on edifice-scale and giant-pockmark measurements.

The second dataset consists of approximately 200 km of single-channel sub-bottom CHIRP profiles acquired with a hull-mounted, 16-transducer Teledyne/Benthos CHIRP III profiler (operating frequency of 2 to 7 kHz; ping rate of 250 to 750 ms; pulse length of 10 ms). These data were processed and interpreted using the GeoSuite 2.6.7 and Kingdom 2025 software packages (automatic gain control, time-variant gain, swell filtering and muting).

Finally, multi-channel seismic reflection profiles with high penetration (approximately 6 s TWTT) but relatively low vertical resolution (10–80 m) were downloaded as PDF files from the VIDEPI Project database [31]. The profiles were assembled according to their line numbers, georeferenced in the WGS84/UTM Zone 33 N coordinate system, and converted to SEG-Y using IMAGE2SEGY [32].

The boundaries of edifices V1–V6 were manually defined at the basal break in slope on the 5 m digital terrain model and its derived slope map. For each polygon, a basal reference surface was generated by interpolating the elevations along the boundary. The base area corresponds to the polygon area, whereas the summit depth corresponds to the minimum water depth; height is the vertical difference between the summit and the basal reference surface; and volume is the positive difference between the digital terrain model and the reference surface within the polygon. The flatness index was calculated as the mean width of the summit terrace (Ws) divided by its mean basal diameter (Wb; FI = Ws/Wb), so higher values identify proportionally broader flat summits. Boundary-dependent parameters remain approximate where talus, erosion or coalescence obscure the basal break; the overlapping basal zone of V2 and V3 was included in both polygons to preserve the geometry of each edifice [6,33].

5. Geology and Geomorphology

5.1. Seismic Stratigraphy and Acoustic Facies

Four main acoustic facies are recognised in the sub-bottom CHIRP profiles and in the previously published multichannel seismic data and are summarised, together with representative colour-rendered seismic panels, in Table 1.

Two features stand out within Facies C. The first is an elongate, asymmetric mounded body interpreted as a contouritic drift (the Elongated Mounded Drift, EM1 in Figure 3), up to about 45 m thick and about 1.2 km wide, which runs sub-parallel to the isobaths and is flanked by two small, elongated moats in a moat–drift–moat configuration. Internally, EM1 shows an aggradational stacking of mounded packages of continuous, moderate- to high-amplitude reflectors, formed by overlapping hemipelagic Upper Pleistocene to Holocene layers of laterally variable thickness that onlap a deeper unit with seismic Facies A (Figure 3). The second consists of concave-upward reflectors forming U-shaped depressions beneath the pockmarks of the western region (Figure 3).

Table 1. Synthesis of the four acoustic facies (A to D) recognised in the sub-bottom CHIRP with representative seismic panels, description and geological interpretation. The colour rendering is a non-calibrated visual transform applied to the original greyscale panels to enhance reflector continuity and facies patterns; colours should not be interpreted as quantitative amplitude values. Original greyscale panels after [3].

Acoustic Facies	Seismic Example	Description	Interpretation
Facies A	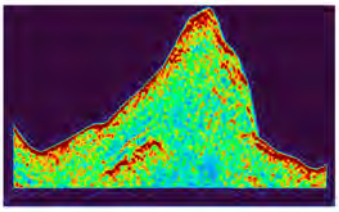	Facies A, the deepest unit, is acoustically semi-transparent to transparent and is bounded at its top by a high-amplitude, discontinuous reflector. It occurs mainly in the western and central–eastern regions, where it locally crops out at the seafloor. Its base and total thickness are not resolved; its top ranges from exposed at the seafloor to buried beneath several tens of metres of Facies C and locally by Facies D.	Carbonate acoustic basement
Facies B	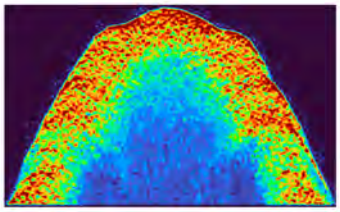	Facies B, mapped only across the eastern region, is an acoustically impenetrable body with a strong upper reflection. It passes laterally into Facies A and is associated with positive-relief features in the eastern region. Its base and total thickness are not resolved because of acoustic impenetrability; its top is locally exposed or overlain by Facies C or D.	Volcanic basement
Facies C	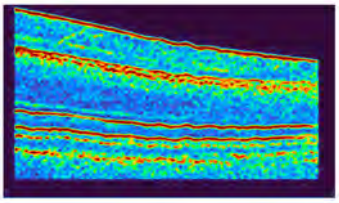	Facies C comprises sub-parallel, high-amplitude, divergent to convergent reflectors with good lateral continuity, alternating with low-amplitude reflectors. It infills basins or drapes flat seafloor areas. It is generally a few to several tens of metres thick and reaches approximately 45 m within EM1.	Upper Pleistocene to Holocene hemipelagic deposits
Facies D	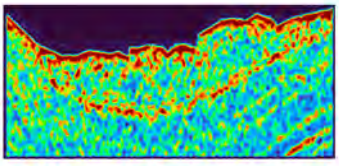	Facies D consists of transparent-to-chaotic, internally reflector-free packages with irregular surfaces. In contrast to the other transparent facies, it is acoustically penetrable, and underlying reflectors can be traced through it. It overlies Facies C and B unconformably. The mapped packages have apparent thicknesses ranging from several metres to about 25 m, depending on the deposit.	Mass-transport deposits (MTDs)

5.2. Geomorphology of the Study Area

The study area lies on the outer continental shelf at about 100 m depth (Figure 1) and upper slope. The seafloor shows an irregular morphology with a clear dichotomy: a jagged eastern sector and a smooth, sediment-dominated western sector, separated by an asymmetric, elongated depression, the Ferdinandea Channel (Figures 2 and 4).

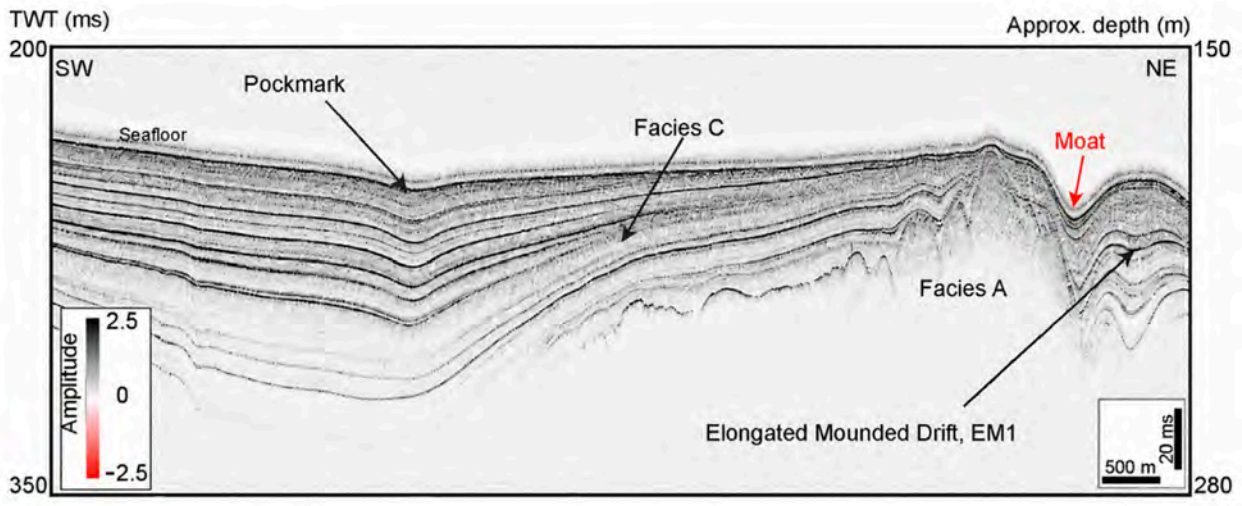

Figure 3. Representative SW–NE sub-bottom CHIRP profile across the western flat region (location in Figure 2). The profile illustrates the principal acoustic facies of the area: Facies C, consisting of sub-parallel, laterally continuous, high-amplitude reflectors that drape and infill the seafloor (interpreted as hemipelagic Upper Pleistocene to Holocene deposits), and the underlying, acoustically semi-transparent Facies A (interpreted as carbonate acoustic basement). A pockmark indents the seafloor in the SW sector as a concave-upward depression rooted below the resolved section, whereas an Elongated Mounded Drift (EM1), an asymmetric, mounded contouritic body, develops within Facies C in the NE sector.

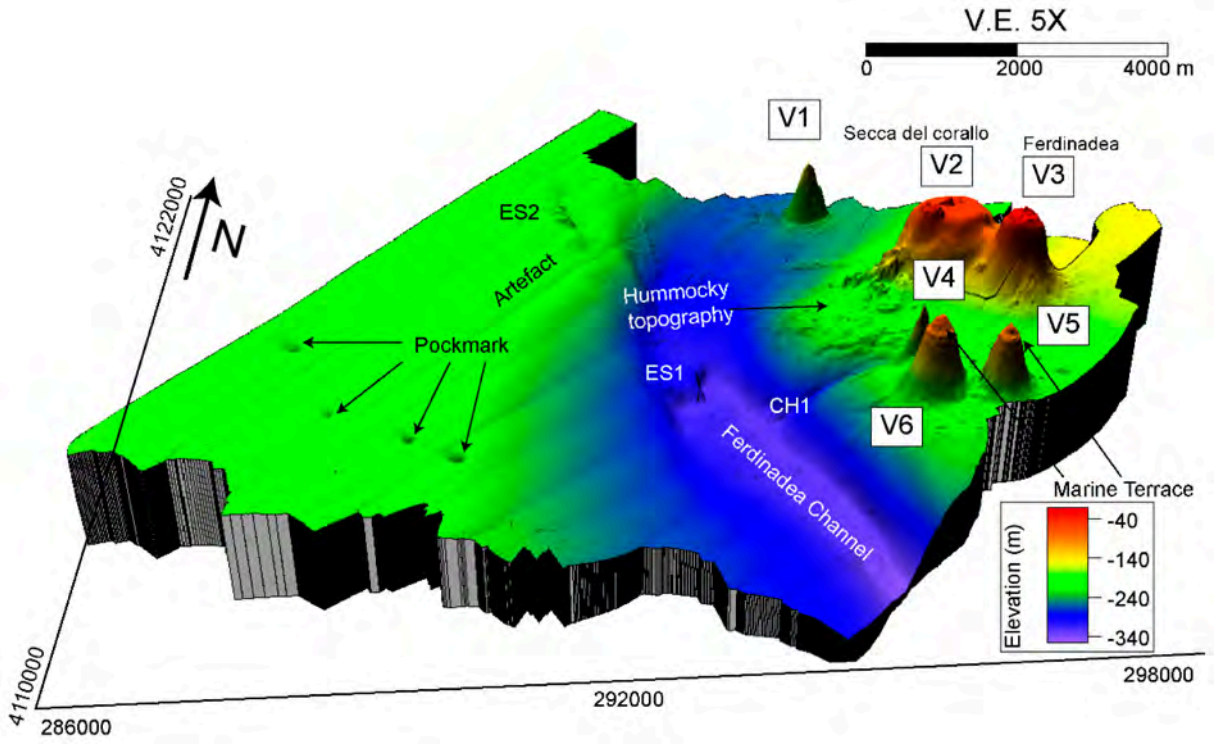

Figure 4. Three-dimensional view of the study area showing its main morphological features: the volcanic edifices (V1 to V6), the Ferdinandea Channel and tributary CH1, the hummocky topography, the erosional surfaces (ES1, ES2), the marine terrace and several pockmarks. The colour scale indicates elevation (in metres); coordinates in UTM Zone 33N (m); vertical exaggeration 5×.

The eastern sector corresponds to the Graham Bank volcanic field and shows a complex seafloor morphology hosting aligned mounds, ridges, and a cluster of volcanic cones. Six volcanic edifices, forming a cluster of small seamounts, have been identified and mapped using multibeam data. Two of them (V2 and V3) display flat summits (Figure 4). Small

gullies, with a shallow incision and limited lateral extent, commonly in spatial association with the mapped scars (Figures 2 and 4), dissect the seafloor and connect the main volcanic cones to the Ferdinandea Channel.

The western sector has a flatter and smoother morphology, with an average slope gradient of 1.2–1.5° that increases westward. The seafloor is punctuated by aligned, normal pockmarks and by steep, NW–SE-trending elongated escarpments (ES1–ES2 in Figure 4).

The central sector corresponds to the Ferdinandea Channel covering an area of about 12 km^2. The channel is an asymmetric, elongate depression about 10 km long and 0.8 to 1.5 km wide, with a predominant N–S to NW–SE (locally NNW–SSE) orientation, deepening from about 200 m at its head to about 350 m southward. The channel also receives a U-shaped tributary, about 1.5 km long and up to 250 m wide, originating from the V4 edifice (CH1 in Figure 4).

5.3. Graham Bank

Two main edifices, V2 and V3 (the latter being the remnant of Ferdinandea Island), coalesce at their bases to form the NW–SE-oriented Graham Bank complex with a major-axis azimuth of N130–N140° (Figure 2). V2, Secca del Corallo, is the largest edifice in the field: it has a circular base, an area of about 2.4 km^2 and a maximum diameter of 1.8 km (Figure 5; Table S1 in Supplementary Material). Prominent reliefs (minimum water depth of 33 m) stand out on its relatively flat top, which forms a terrace at a present-day water depth from 50 to 60 m. The summit reliefs have seismic Facies B (Table 1). Below the edge of the summit terrace, a second, more developed terrace 200 to 300 m wide occurs at 100 to 115 m on the southeastern side of the edifice.

The northern flank hosts an elliptical volcanic depression about 500 m long (Figure 6), with walls dipping up to 20°, that encloses a mound up to 13 m high and 160 m wide. The mound is interpreted as the site of focused fluid escape as witnessed by water-column hydroacoustic anomalies in the sub-bottom profiles (Inset Figure 6). Across the broader volcanic field, isolated, clustered and aligned mounds up to 5 to 10 m high, trending NW–SE and NNW–SSE, form a hummocky topography on the western and southwestern flanks of Graham Bank (Figure 5).

The Ferdinandea edifice (V3) is a truncated cone rising approximately 150 m above the surrounding seafloor, with an elliptical base and a major axis exceeding 1.4 km (Figure 2; Table S1 in Supplementary Material). Its uneven summit surface displays sub-concentric ridges and furrows that extend downslope from the top. Dredging by Micallef et al. (2024) [4] indicates that the ridges are built of pyroclastic material, including scoriaceous lapilli, palagonitised tuff and agglutinated clasts rather than coherent lava. Outward from the summit terrace, the seafloor passes to a flat to gently sloping surface (<4°), interpreted as a wave-reworked depositional terrace, below which the slope steepens sharply (Figure 5). This terrace is up to 70 m wide in the NW and SE sectors and narrows to 30 m in the NE and SW; its edge lies at 40 to 43 m in the northern and eastern sectors and shallows to 36 to 38 m to the south and west. The flanks of the edifice are very steep (up to 25°, the highest in the field) and remarkably regular, lacking gullies or erosional scars, and no lava flows occur along the slopes or around the base.

Unlike the flat-topped V2 and V3 edifices, edifices V1, V5 and V6 are characterised by a conical morphology, with steep, regular flanks that rise from the surrounding seafloor to a well-defined summit (Table S1 in Supplementary Material, Figure 4). However, V5 and V6 depart from a purely conical form, inasmuch they develop a terraced surface at about 95 m depth, which interrupts the continuity of the flanks and marks a distinct break in slope along the edifice profile. Finally, V4 represents a well-preserved, regular conical edifice. It is a steep-sided volcano rising approximately 124 m above the surrounding seafloor, from a

base at about 232 m water depth to a pointed summit at approximately 108 m. Its nearly circular basal outline, among the smallest in the volcanic field, together with the absence of a summit terrace, confirms its well-preserved conical morphology (Figure 7; Table S1 in the Supplementary Material). The cone emerges abruptly from the surrounding floor through a sharp increase in gradient at the base and displays a markedly asymmetric profile, with a steeper flank facing the Ferdinandea Channel and a saddle at its southern base bordered by an annular ridge (Figure 8), interpreted as the remnant of an older and larger edifice.

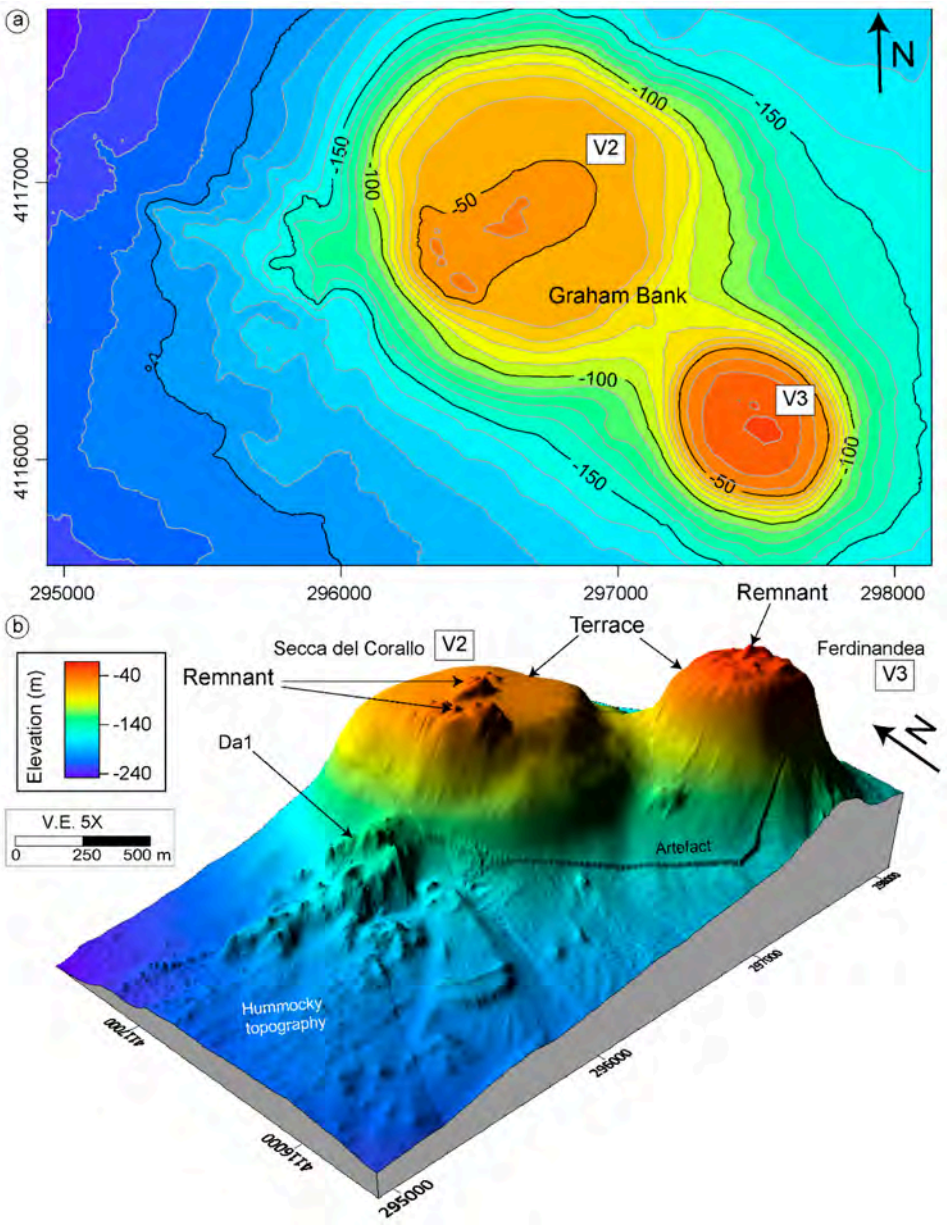

Figure 5. Detailed bathymetry of the coalescent V2–V3 complex (Graham Bank), the shallowest edifices of the field. (**a**) Shaded-relief bathymetric map with superimposed depth contours (10 m interval; bold, labelled contours every 50 m) showing the flat, wave-truncated summits of V2 (Secca del Corallo) and V3 (Ferdinandea edifice) and their NW–SE coalescence. (**b**) Perspective 3D shaded-relief view (looking approximately N) of the same area, highlighting the wave-cut summit terraces of both edifices, the 9 m deep summit of V3 (the shallowest point of the entire field), the hummocky topography on the lower SW flank, and a linear acquisition artefact. Coordinates in UTM Zone 33N (m); vertical exaggeration 5×.

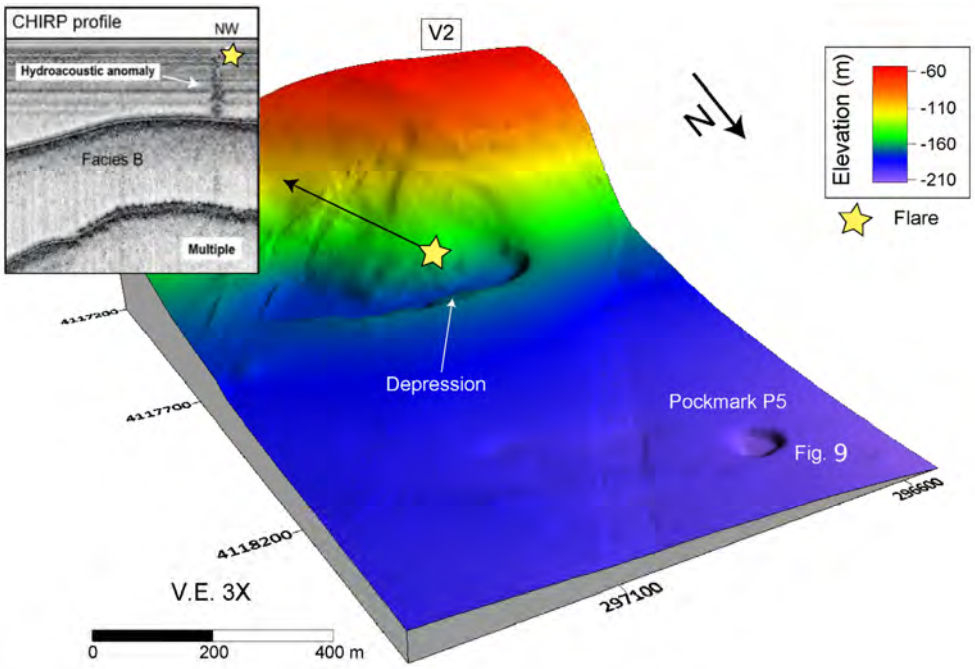

Figure 6. Three-dimensional view (vertical exaggeration 3×, looking approximately SW) of the flank of the V2 edifice (Secca del Corallo). On the upper flank, a sub-circular depression is associated with a water-column hydroacoustic anomaly interpreted as an active gas flare (yellow star), marking focused fluid escape from the edifice, whereas a well-defined pockmark indents the gently sloping plateau to the SE. Coordinates in UTM Zone 33N (m).

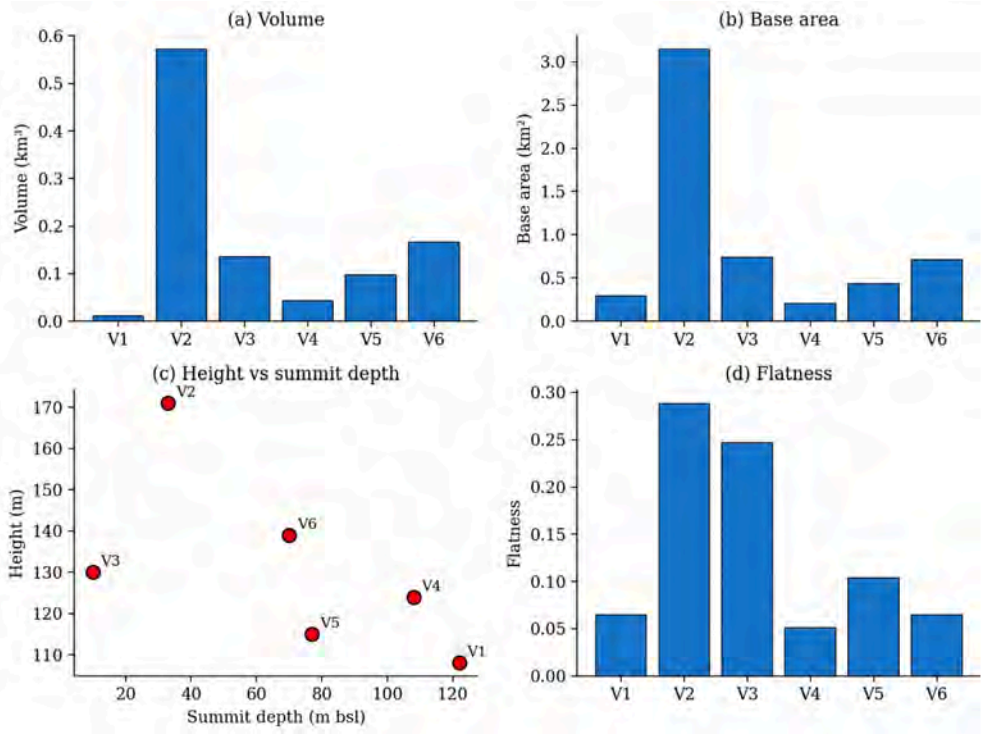

Figure 7. Morphometric parameters of the six volcanic edifices (V1 to V6): (**a**) volume; (**b**) base area; (**c**) height versus summit depth; (**d**) flatness index. The flat-topped edifices V2 and V3 are distinguished from the conical edifices V1, V4, V5 and V6.

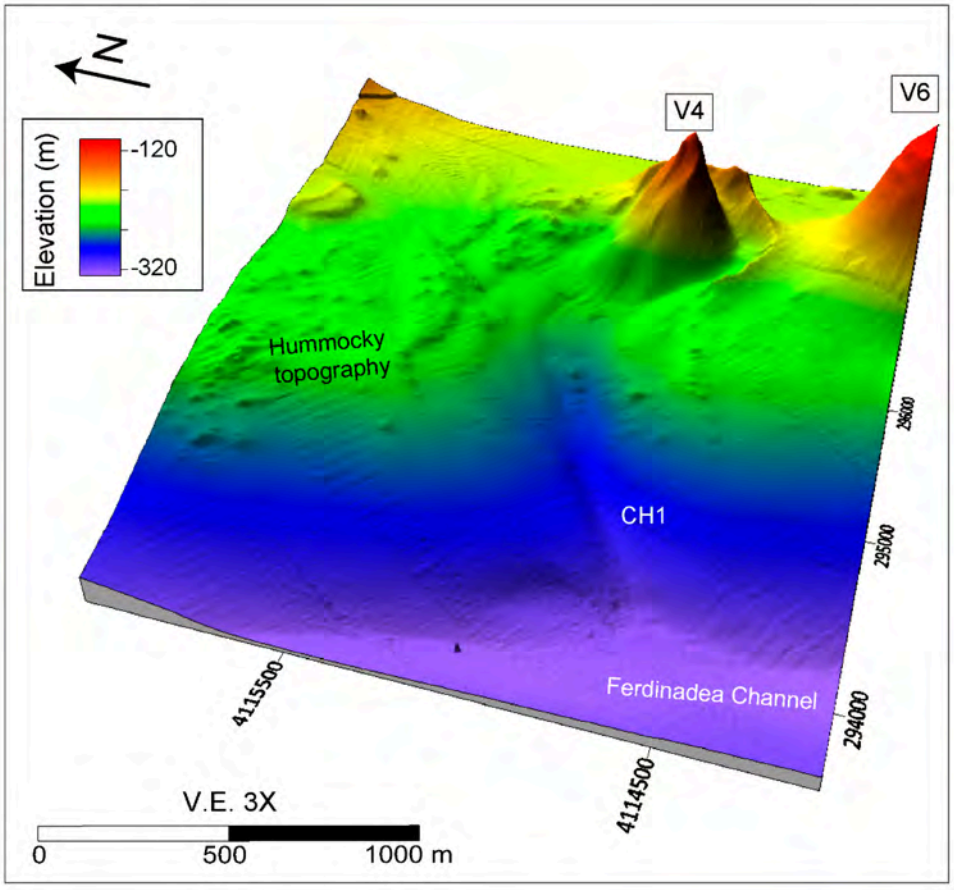

Figure 8. Detailed perspective 3D view of the central study area showing the volcanic edifices V4 and V6, the Ferdinandea Channel, CH1 and the hummocky topography. V4 and V6 display the steep, regular flanks typical of the conical edifices of the field, and the asymmetric profile of V4 is well expressed. The colour scale indicates elevation (in metres); coordinates in UTM Zone 33N (m); vertical exaggeration 3×.

5.4. Pockmarks

Apart from the volcanic edifices, pockmarks are among the most distinctive features of the area. They are classified from the major-axis distribution, which shows a clear gap: features with major axes > 250 m were assigned to the giant class, whereas those ≤ 130 m were assigned to the normal class; no features occur between 130 and 250 m. Internal depth was therefore used as a descriptive parameter rather than as a classification threshold (Table S2 in Supplementary Material). Seventeen pockmarks were mapped in the high-resolution survey: ten smaller, sub-circular depressions (axes about 45 to 130 m, depths 2 to 12 m), occurring as isolated, clustered or, in a few cases, NW–SE-aligned features within the Ferdinandea Channel. Six larger sub-circular pockmarks are present on the flat western plateau, with axes up to 540 m and depths up to 22 m, and one (P5 in Figure 9) is located in the eastern sector (Table S2 in Supplementary Material). P5 is immediately north of the V2 edifice and is one of the largest features of the normal population: it is about 120 m wide and indents the gently sloping seafloor by roughly 8 to 10 m, showing a flat floor bounded by walls that steepen on the northeastern side (Figure 9).

The normal pockmarks are more circular and concentrate in the deepest part of the area, whereas the giant pockmarks are more elliptical and occur at shallower depths. This distribution is attributed to differences in sediment lithology and texture and in the thickness of the hemipelagic cover available for pockmark formation. Throughout the western part of the study area, characterised by seismic facies C, indicative of a relatively thick sedimentary cover, the pockmarks display continuous, high-amplitude, concave-

upward reflectors, indicating formation by sediment collapse and root area below the sub-bottom profiler penetration depth (Figure 3). The surface-area distribution (Figure 10a) is dominated by the giant pockmarks P16 and P4, up to two orders of magnitude larger than the normal pockmarks of the Ferdinandea Channel. The plot of major against minor axis (Figure 10b) defines a continuous, near-linear trend in which the giant population (axes > 250 m) plots at the upper end, whereas the normal population clusters below about 130 m. The internal-depth distribution (Figure 10c) shows that the giant pockmarks are also the deepest (up to 22 m for P3), whereas most normal pockmarks are 2 to 6 m deep. The summit-depth distribution (Figure 10d) separates the two populations by water depth: the giant pockmarks occupy the shallow western plateau (about 190 to 220 m), while the normal pockmarks occupy the deeper floor of the Ferdinandea Channel (about 280 to 330 m).

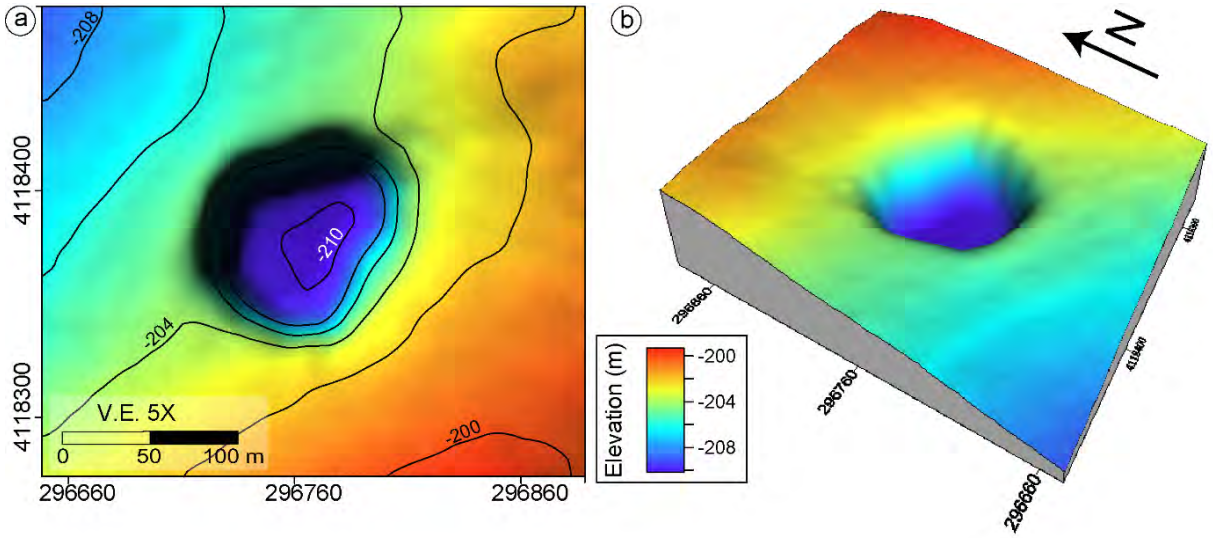

Figure 9. Detail of a sub-circular pockmark on the eastern sector (P5; location in Figure 2). (**a**) Shaded-relief bathymetric map with isobaths (2 m contour interval, from −200 to −210 m). (**b**) Perspective 3D view (looking approximately SW) of the same feature, showing the smooth, undisturbed seafloor surrounding the pockmark morphology. Coordinates in UTM Zone 33N (m); vertical exaggeration 5×.

5.5. Mass-Transport Deposits

Eleven mass-transport deposits, distributed across the study area, fall into four types (debris avalanches, rockfalls, slumps/debris flows and channelised deposits), each with a distinctive morphological and seismic signature, and differ in volume, deposit area, planform dimensions and mean slope (Table S3 in Supplementary Material).

Debris avalanche deposits result from relatively large-scale failures associated with volcanic flank instability; they are characterised by jagged seafloor and blocky topography and by transparent to chaotic seismic facies with discontinuous, very low-amplitude reflectors and low internal coherence (seismic Facies D). The most prominent example is the DA1 deposit (~2.15 km^2), located at the base of the western flank of V2. It displays detached blocks downslope from an amphitheatre scar with slopes up to 21° and records gravitational adjustment of young volcanic material (Figure 11). Rockfalls form smaller, isolated clusters of heterometric blocks with hummocky seafloor topography at the foot of the steep flanks of the volcanoes (e.g., V1 and V3 in Figure 11), as well as at the base of the steep fault escarpments (e.g., ES1 in Figure 11). Slumps and debris flows, which involve the failure of stratified sediments, display rotational geometries with a chaotic seismic character: SD1 forms a hummocky body of about 0.9 km^2, while SD3 forms an arcuate body of 0.75 km^2 at the foot of fault escarpments (Figure 11).

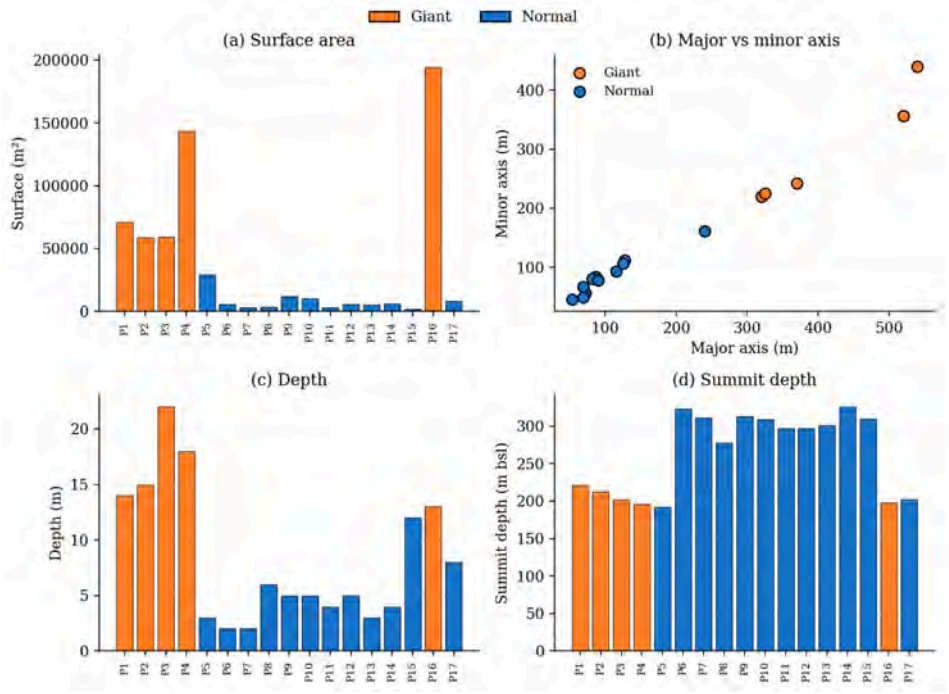

Figure 10. Morphometric parameters of the seventeen mapped pockmarks, distinguishing the normal and giant populations: (**a**) surface area; (**b**) major versus minor axis; (**c**) internal depth; (**d**) summit (water) depth. The giant pockmarks of the western plateau are systematically larger, deeper and shallower-seated than the normal pockmarks of the Ferdinandea Channel.

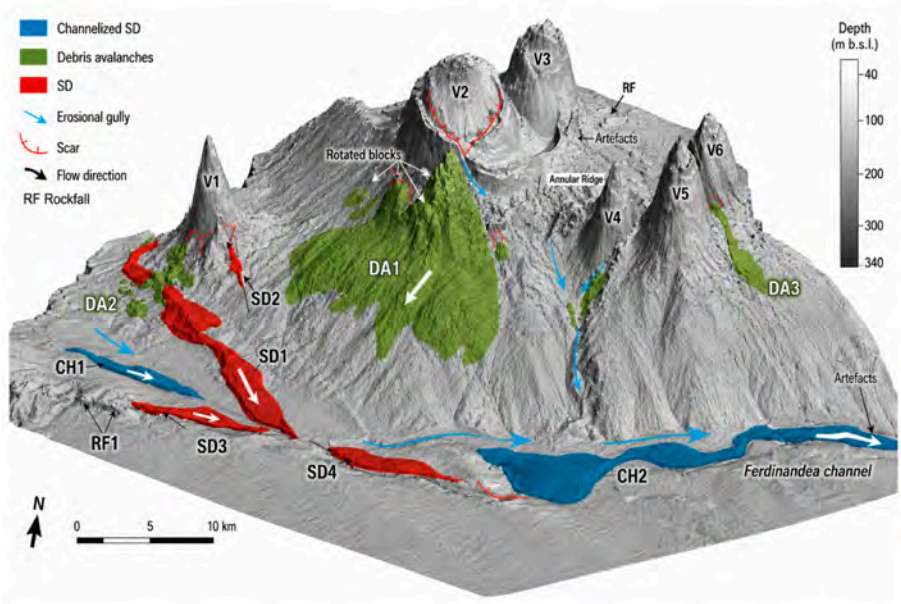

Figure 11. Perspective 3D shaded-relief view (looking approximately N) of the Graham Volcanic Field, showing the volcanic edifices (V1 to V6) and the mass-transport inventory mapped on the multibeam bathymetry. Deposits are distinguished by colour: volcanic-rock avalanches in green (DA1 to DA3), slump and debris-flow deposits in red (SD1 to SD4, with the rockfall RF1) and channelised deposits in blue (CH1, CH2), routed along the Ferdinandea Channel. The largest debris avalanche (DA1), sourced from the V2 to V3 complex, shows rotated blocks and an amphitheatre scar, whereas V2 and V3 bear wave-cut marine terraces and V4 a truncated crater with an annular ridge. Arrows and symbols mark gullies, normal faults, scars and flow directions; labelled artefacts are acquisition or processing features of the data (modified from Basilone et al. 2026 [34]).

Channelised deposits occupy structural depressions and show mounded, hummocky facies with chaotic seismic signals. CH1 (~0.96 km^2) has U- to V-shaped channel mor-

phologies and downslope gradients of 1 to 2°, whereas CH2 (~2.46 km^2) occupies the southernmost sector of the Ferdinandea Channel with a flat thalweg (gradient below 1°) and channel walls of 4 to 7° (Figure 12). Across the field, isolated heterometric blocks up to 10 m high are scattered along the flanks and toes of the largest cones, as far as 1 km from the edifices, and record additional debris-avalanche and rockfall activity.

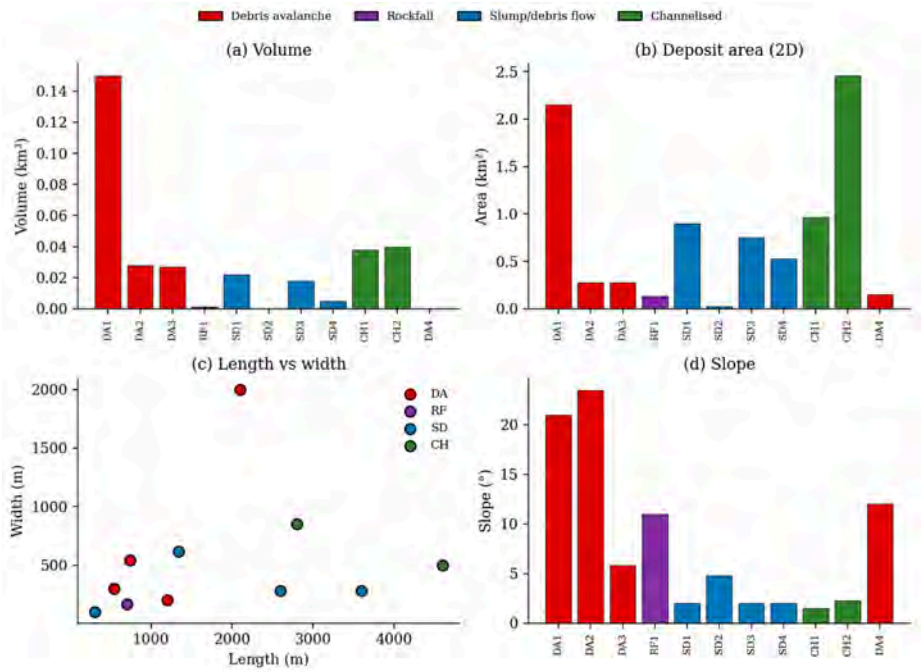

Figure 12. Morphometric parameters of the mapped mass-transport deposits: (**a**) volume; (**b**) deposit area; (**c**) length versus width; (**d**) slope. Symbols are grouped by deposit type (debris avalanche, rockfall, slump or debris flow, channelised). The debris avalanche DA1 and the channelised deposit CH2 are the largest bodies.

6. Discussion

6.1. Geological and Geomorphic Evolution of the Graham Bank Volcanic Field

The geomorphic evolution of the present-day seafloor at the Graham Bank volcanic field reflects the long-term interaction among tectonic deformation, volcanism, fluid flow, bottom-current reworking and gravitational instability (Figure 13). These processes should not be regarded as independent, because they are ultimately controlled by the structural framework of the Sicily Channel Rift [20,35].

The tectonic setting is the fundamental control on the development of the volcanic field. The distribution and orientation of the volcanic edifices indicate that magma ascent was strongly guided by inherited N–S and NW–SE to WNW–ESE structures. The N–S arrangement of the main volcanic centres is consistent with the regional Capo Granitola–Sciacca Fault Zone, whereas the NW–SE orientation of several cone bases, vent alignments, pockmark clusters and sedimentary lineaments reflects the influence of the main extensional structures of the Sicily Channel Rift [4,20,36]. The morphology of the Ferdinandea and the surrounding cones suggests that the field developed through repeated localised eruptions rather than through the sustained growth of large polygenetic volcanoes [13,33,37,38]. Their limited volumes and the predominance of fragmental deposits, as implied by the early accounts of the Ferdinandea eruption, point to a prevalence of explosive activity in the building of the volcanoes. We thus suggest the volcanic edifices were probably emplaced during relatively short-lived monogenetic eruptive episodes, dominated by explosive magma–water interaction with the magmatic plumbing system mainly controlled by the

regional structural framework. This structural reading is independently corroborated by regional magnetic potential-field data: the magnetic-anomaly map of the NW Sicily Channel resolves the surface volcanism around Graham Bank [20], and the Bouguer-anomaly map of Sicily shows a gravimetric high over the same region [39].

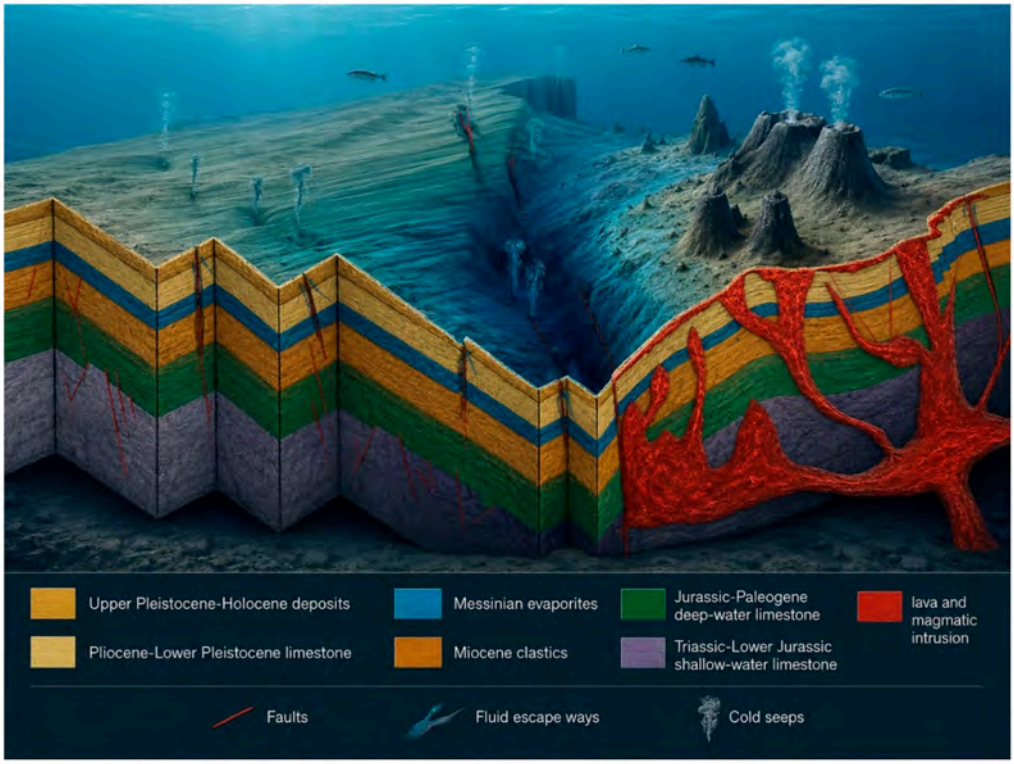

Figure 13. Conceptual geological model of the Graham Bank area, showing the stratigraphic succession (Triassic to Lower Jurassic shallow-water limestone, Jurassic to Paleogene deep-water limestone, Miocene clastics, Messinian evaporites, Pliocene to Lower Pleistocene limestone and Upper Pleistocene to Holocene deposits), the fault network, the magmatic intrusion feeding the Graham Bank edifices, and the fluid-escape system (faults, fluid-escape pathways, cold seeps and focused seepage plumes). Modified from Spatola et al. (2018) [3] by using ChatGPT-5.5.

The cones were built mainly of poorly consolidated pyroclastic material, rapidly exposed to wave erosion, marine reworking and gravitational degradation. This is clearest at Ferdinandea, whose brief emergence in 1831 was only a transient subaerial stage within a much longer history of submarine construction and dismantling. Dredging corroborates this interpretation. The freshest deposits come from the summit terrace of the Ferdinandea edifice (V3). They consist of loose, poorly sorted scoriaceous sand and gravel, subangular clasts of palagonitised tuff, and blocks ranging from highly vesicular and fluidal scoria to bread-crusted and agglutinated lava, all consistent with explosive activity. On the contrary, in the deeper, more degraded cones, dredges yielded surficial carbonate concretions and mud, together with lithified blocks of angular vesicular clasts in a carbonate-mud matrix, interpreted as reworked post-eruptive deposits and indicating a well-developed carbonate drape [4]. This gradient, from fresh pyroclasts on the youngest cone to carbonate-draped material on the older ones, matches the seafloor backscatter distribution, in which cone tops and flanks return high values that peak at V3 [4]. The contrast in flatness index between the two groups therefore separates the edifices by evolutionary stage, not necessarily by eruptive style. Overall, V4 may represent the clearest example of volcanic edifice degradation in the study area, with its morphology more likely reflecting a westward-

breached summit depression and associated lobate avalanche deposit, later reoccupied by an inner cone, rather than repeated flank-retreat events.

The alignment of pockmarks, hydroacoustic flares and focused seepage zones along NW–SE and NNW–SSE lineaments indicates that the structural fabric also regulates fluid discharge at the seafloor [40]. A similar control has been observed on the Pelagian shelf [41–43]. In the absence of direct gas or pore-fluid analyses, the source of the fluids cannot be resolved. Plausible options include a magmatic or hydrothermal component related to the cooling volcanic system, thermogenic hydrocarbons generated in deeper sedimentary units, biogenic methane from shallow organic-rich deposits, and diagenetic fluids expelled during compaction [7]. These end members may occur separately or as mixtures; a composite, structurally focused fluid-flow system therefore remains a hypothesis requiring geochemical testing (Figure 13). Physical evidence for such focused discharge has been recovered from the field: a dredge on the NE flank of V2, close to the large basal pockmark where gas venting had previously been observed, retrieved intact chimney-like structures, elongate amalgamations of indurated volcaniclastic sand and scoriaceous gravel bound by a reddish-brown to yellow matrix and traversed by a central conduit less than 1 cm across, consistent with fluid- and gas-focused cementation at the seafloor [4]. The giant pockmarks of the western plateau developed where Facies C, interpreted as hemipelagic or volcanogenic sedimentary cover, is thickest and record repeated or prolonged expulsion, whereas the smaller pockmarks of the Ferdinandea Channel formed in areas with a thinner sedimentary coverage and were probably reshaped during episodic discharge, in agreement with the size–substrate relationships described for pockmark fields worldwide [40] and across the Mediterranean [44]. The persistence of active water-column flares above the volcanic depression and vents further supports the interpretation that seepage remains active today and structurally controlled [44,45].

The long-term evolution of the volcanic field was also strongly influenced by bottom-current activity, particularly across the western sedimentary sector. The occurrence of the elongated mounded drift EM1 indicates that contour-parallel currents have actively reworked the uppermost sedimentary cover during the Late Pleistocene to Holocene [46,47]. Its external and internal geometry suggest persistent along-slope sediment transport, probably linked to the regional circulation of Mediterranean water masses through the Sicily Channel [19,48]. Bottom currents likely contributed to the redistribution of volcaniclastic and hemipelagic sediment around the volcanic edifices, promoting localised erosion and deposition. Their role was therefore not limited to smoothing the volcanic relief but included the development of sedimentary bodies with variable thickness, grain size and internal strength. Such current-reworked deposits may have contributed to slope instability by creating weakly consolidated accumulations adjacent to volcanic scarps, fault-controlled depressions and seepage zones.

Mass-wasting processes also shape the Graham Bank volcanic field. The widespread occurrence of debris avalanches, rockfalls, debris flows, slumps and channelised deposits indicates that both volcanic and sedimentary slopes remain prone to recurrent gravitational adjustment. Instability is favoured by the steep gradients of the volcanic edifices, which locally approach the angle of repose for unconsolidated volcaniclastic material and by the poor cohesion of the pyroclastic deposits [49]. In this context, volcanic construction created the topographic relief and weak material required for failure, while faulting and fluid seepage progressively reduced slope stability and channelised sediment transport towards the surrounding depressions and channels [50]. The spatial pattern of the mass-wasting deposits reflects a twofold character of seafloor instability and collapse. Failures rooted on the volcanic flanks (DA1 to DA3, RF1) involve coarse, cohesionless volcaniclastic material and travel short distances on the steepest gradients, whereas the slumps, debris flow and

channelised bodies of the central to western sector mobilise stratified, water-saturated sediment on much gentler slopes and are routed for kilometres along the Ferdinandea Channel. This partition between source-controlled and route-controlled mass wasting matches that described on other continental margins [51] and in other Mediterranean basins [52].

The mapped mass-transport deposits indicate that instability in the Graham Bank area results from the combined action of several preconditioning and triggering factors. Faults and fractured zones may provide preferential detachment surfaces, while fluid seepage can reduce effective stress by increasing pore-fluid pressure within volcaniclastic and sedimentary deposits. Bottom-current reworking may further contribute through the redistribution of unconsolidated sediment and local erosion or accumulation processes near slope breaks. Episodic seismic shaking and wave loading may act as additional triggers, particularly in the shallowest sectors of the volcanic field [53,54].

Since the failures of the Graham Bank volcanic field affect monogenetic cones and are confined to shallow-water environments, they are much smaller than those documented around major oceanic islands. However, they share similar controlling mechanisms with their giant counterparts affecting polygenetic, composite high-relief oceanic volcanoes. They occur on steep volcanic flanks, with a prevalence of weak pyroclastic material, are controlled by structural discontinuities and are associated with active fluid circulation. The largest mapped body, DA1, involves about 0.150 km^3, several orders of magnitude less than the giant flank collapses of the Canary islands [55,56], but of the same order as the recurrent failures documented on active Mediterranean edifices such as Stromboli, where even modest submarine landslides are regarded as potentially tsunamigenic because they occur in shallow water. At Graham Bank, the very shallow summits of V3 and V2 (9 and 33 m) would place any future failure of the upper flanks close to the sea surface, where the efficiency of wave generation is the highest [53].

Geodetic monitoring at Surtsey documented decelerating subsidence, from 15–20 cm yr^{-1} immediately after the eruption to 1–2 cm yr^{-1} by 1991 [57]. A similar post-eruptive adjustment may have affected Ferdinandea, but no geodetic time series exists for the bank; repeated hydrographic and multibeam surveys record only the combined morphological change. Historical observations indicate rapid destruction of the emergent island in 1831, while hydrographic surveys placed the shallowest point at ~3 m below sea level in 1883, ~8 m in 1914 and ~9 m in 2012–2015 [6,8,16]. Thus, the directly observed post-1883 lowering of the shallowest point is approximately 6 m, subject to metre-scale uncertainty due to differences among survey methods and vertical-reference conventions. The 25–28 m-deep summit terrace instead records spatially distributed wave abrasion and must not be equated with 28 m of measured summit lowering. The separate contributions of wave erosion, cooling-related subsidence and gravitational adjustment cannot be quantified from the available data.

Wave erosion was strongest during the early post-eruptive stage and then decelerated as the edifice deepened and more resistant feeder-dyke and palagonitised-tuff materials were exposed [58]. The North Atlantic analogues show faster vertical lowering: Surtla was eroded to ~45 m below sea level within 18 years (~2.5 m yr^{-1}) and to ~51 m after a further 26 years (~0.23 m yr^{-1}) [13,59]. Jólnir and Syrtlingur, which reached ~70 m above sea level, had summit terraces at ~43 and ~34 m below sea level by 2007, corresponding to long-term average lowering rates of approximately 2.5–2.8 m yr^{-1}, although much of this change occurred during the initial rapid destruction of the emergent cones [59]. By comparison, the post-1883 lowering of Ferdinandea's shallowest point averages ~0.05 m yr^{-1}. This contrast is consistent with a shallower effective wave-erosion level under the less energetic

Mediterranean wave climate, while recognising that the compared rates refer to different phases and geomorphic markers.

The wave-reworked terrace of V3 provides a local constraint on the depth of effective wave reworking: its edge lies at 40 to 43 m on the northern and eastern sides but shallows to 36 to 38 m in the south and west, recording deeper erosion on the flanks most exposed to the dominant storms. Seen as relative sea-level markers, the wave-cut terraces also carry a chronological message: the deeper terraces of V2 (50 to 60 m and 100 to 115 m) cannot be explained by the present-day wave climate and are best interpreted as planation surfaces cut when the sea level stood lower, during the stillstands that punctuated the post-LGM transgression [60]. The Graham Bank edifices therefore predate the 1831 event by at least several millennia, and the Ferdinandea eruption rejuvenated only the shallowest cone of a much older, Late Pleistocene to Holocene edifice. The rapid disappearance of the island thus reflects the combined action of wave erosion of unconsolidated deposits, cooling-related subsidence and gravitational adjustment following rapid loading [61]; regional extension along the Sicily Channel Rift may represent an additional, less directly constrained contribution [62].

6.2. Geohazard Implications and Future Perspectives

The Ferdinandea system combines several conditions that make slope failure a tangible geohazard. The young volcanic edifices are poorly consolidated and have steep flanks reaching ~25°, locally approaching the angle of repose, while elevated pore-fluid pressures and active fluid seepage along fault-controlled pathways further reduce slope stability. Although most mapped mass-transport deposits are small, the combination of steep slopes, weak material, active seepage and documented local seismicity indicates that larger failures cannot be excluded; however, this inference requires dedicated geotechnical and slope-stability analyses. The exposure to risk is not restricted locally. The summit of V3 lies about 9 m below sea level along routes with heavy maritime traffic, and the bank is a documented hazard to navigation [16]. A partial collapse of the shallow flanks, although of limited volume, could generate locally significant waves, whose coastal impact requires dedicated failure and tsunami modelling [53]. Ongoing water-column flares indicate active fluid discharge and warrant monitoring, especially because renewed eruptive or hydrothermal activity would affect the ecological value of the bank, which hosts red coral colonies and other sensitive benthic communities [20]. In addition, it serves as a major spawning ground for small pelagic fish [63]. Moreover, the area is characterised by intense maritime traffic and the presence of submarine cables and pipelines [64,65].

Short-term priorities are repeat high-resolution multibeam surveys to quantify morphological change, scarp-retreat rates and the evolution of depositional lobes, together with geochemical analyses of pore fluids and gas samples to discriminate among their possible magmatic/hydrothermal, thermogenic, biogenic and diagenetic sources. Medium-term priorities are systematic geotechnical sampling to constrain shear strength, consolidation and pore pressure, followed by geomechanical slope-stability modelling that incorporates in situ properties, pore-pressure distributions and seismic-loading scenarios. Long-term objectives include isotopic dating and palaeoseismic investigations to refine the mass-wasting chronology and correlate it with documented seismicity, and integrated geodynamic simulations coupling tectonic, magmatic, oceanographic and surface processes.

7. Conclusions

The present-day morphology of the Graham Bank volcanic field is best read as the combined work of volcanism, tectonic deformation, fluid escape, mass-wasting and bottom-current reworking. The relict of the 1831 eruption is the shallowest cone (~−9 m) of a

volcanic field of six edifices, and the fault-controlled Ferdinandea Channel divides the area into a volcanic eastern sector and a sedimentary western one.

Ferdinandea itself yields an unusually well-dated record of post-eruptive decay. The island reached approximately 60 m above sea level in 1831 and disappeared within months; later hydrographic observations record a change in the shallowest point from ~3 m below sea level in 1883 to ~9 m in 2012–2015. This comparison documents approximately 6 m of further lowering since 1883, whereas the 25–28 m-deep summit terrace records broader wave abrasion. The available data do not allow the observed change to be partitioned quantitatively among erosion, cooling-related subsidence and gravitational adjustment. The geometry of the terraces suggests repeated late-Quaternary planation, although correlation with individual sea-level stillstands requires independent chronological control; the 1831 eruption provides an absolute historical anchor.

Activity continues today. An extensive fluid-escape system of normal and giant pockmarks, gas chimneys and water-column flares follow the NW–SE and NNW–SSE faults, showing that tectonic structure strongly influences the location of fluid emission at the seafloor. In the absence of geochemical analyses, magmatic/hydrothermal, thermogenic, biogenic and diagenetic sources remain possible options, which could also operate in conjunction. Mass wasting is equally widespread, from debris avalanches and rockfalls on the volcanic flanks to slumps, debris flows and channelised bodies routed along the faults. Most of these deposits are small, yet the young edifices are only marginally stable, with slopes near the angle of repose. Due to high pore-fluid pressures and the documented seismicity, larger failures remain possible, although their probability and magnitude require dedicated geotechnical constraints. Such failures are best read as the product of several superimposed triggers rather than of tectonics alone. These results also have practical relevance. Graham Bank is a biodiversity hotspot and a major anchovy spawning ground, and it is crossed by heavy maritime traffic and by submarine cables and pipelines.

Overall, the present seafloor of Graham Bank records the superposition of processes acting at very different rates. Tectonics initially controlled the location and orientation of the edifices, while volcanism generated the relief and the low-strength volcaniclastic material that made the field inherently susceptible to erosion and failure. The same structures subsequently guided fluid migration and seepage, bottom currents redistributed sediment across the western plateau, and gravitational processes progressively dismantled the edifices. Tectonics and volcanism thus set the template over millennial timescales, wave erosion and thermal subsidence dominated the decades following 1831, and fluid escape, bottom currents and mass wasting operate today. Graham Bank should therefore be regarded as an actively evolving submarine landscape, and Ferdinandea as an unusually compact template for reading the growth, decay and hazard potential of shallow submarine monogenetic volcanoes elsewhere.

Supplementary Materials: The following supporting information can be downloaded at https://www.mdpi.com/article/10.3390/jmse14161460/s1. Table S1: Morphometry of the Volcanic edifices. Table S2: Morphometry of Pockmarks. Table S3: Morphometry of the Mass-Transport deposits.

Author Contributions: Conceptualisation, D.S. and L.B.; methodology, D.S. and L.B.; formal analysis, D.S. and L.B.; data curation, D.S. and L.B.; writing, original draft preparation, L.B. and D.S.; writing, review and editing, D.S., L.B., F.G., F.L.C., G.B. and A.S. All authors have read and agreed to the published version of the manuscript.

Funding: This research received no external funding.

Data Availability Statement: Bathymetric and sub-bottom profile data can be consulted by contacting the corresponding author: D.S. (daniele.spatola@uniroma1.it).

Acknowledgments: The oceanographic survey benefited from funding provided through the RITMARE project (CNR Mazara del Vallo, Capo Granitola section, resp. G. Basilone) and MIUR and University of Palermo funds (PJ_AUTF_008539, resp. A. Sulli). All participants and technical staff of the oceanographic cruises are gratefully acknowledged for their contribution to the research. We are gratefully to the Editor and to the five anonymous reviewers.

Conflicts of Interest: The authors declare no conflicts of interest.

References

1. Argnani, A. The strait of sicily rift zone: Foreland deformation related to the evolution of a back-arc basin. *J. Geodyn.* **1990**, *12*, 311–331. [CrossRef]
2. Corti, G.; Cuffaro, M.; Doglioni, C.; Innocenti, F.; Manetti, P. Coexisting geodynamic processes in the Sicily Channel. *Spec. Pap.-Geol. Soc. Am.* **2006**, *409*, 83.
3. Spatola, D.; Micallef, A.; Sulli, A.; Basilone, L.; Ferreri, R.; Basilone, G.; Bonanno, A.; Pulizzi, M.; Mangano, S. The Graham Bank (Sicily Channel, central Mediterranean Sea): Seafloor signatures of volcanic and tectonic controls. *Geomorphology* **2018**, *318*, 375–389. [CrossRef]
4. Micallef, A.; Geldmacher, J.; Watt, S.F.L.; Ferrante, G.M.; Ford, J.; Lodolo, E.; Civile, D.; Hodgetts, A.G.E.; Felgendreher, M.; Licari, J.G. Submarine volcanism in the Sicilian Channel revisited. *Mar. Geol.* **2024**, *474*, 107342. [CrossRef]
5. Gemmellaro, C. *Relazione dei Fenomeni del Nuovo Vulcano: Sorto dal Mare fra la Costa di Sicilia e L'isola di Pantelleria nel Mese di Luglio 1831*; Pastore: Catania, Italy, 1831.
6. Cavallaro, D.; Coltelli, M. The Graham volcanic field offshore southwestern Sicily (Italy) revealed by high-resolution seafloor mapping and ROV images. *Front. Earth Sci.* **2019**, *7*, 311. [CrossRef]
7. Coltelli, M.; Cavallaro, D.; D'Anna, G.; D'Alessandro, A.; Grassa, F.; Mangano, G.; Patanè, D.; Gresta, S. Exploring the Submarine Graham Bank in the Sicily Channel. *Ann. Geophys.* **2016**, *59*, S0208. [CrossRef]
8. Spatola, D.; Sulli, A.; Basilone, L.; Casalbore, D.; Napoli, S.; Basilone, G.; Chiocci, F.L. Morphology of the submerged Ferdinandea Island, the 'Neverland' of the Sicily Channel (central Mediterranean Sea). *J. Maps* **2023**, *19*, 2243305. [CrossRef]
9. Dean, D.R. Graham Island, Charles Lyell, and the craters of elevation controversy. *Isis* **1980**, *71*, 571–588. [CrossRef] [PubMed]
10. Washington, H.S. ART. VIII.—The Submarine Eruptions of 1831 and 1891 near Pantelleria. *Am. J. Sci. (1880–1910)* **1909**, *27*, 131. [CrossRef]
11. Carapezza, M.; Ferla, P.; Nuccio, P.M.; Valenza, M. Caratteri petrologici e geochimici delle vulcaniti dell'Isola Ferdinandea. *Rend. Soc. Ital. Mineral. Pet.* **1979**, *35*, 377–388.
12. Németh, K.; Kósik, S. Review of Explosive Hydrovolcanism. *Geosciences* **2020**, *10*, 44. [CrossRef]
13. Kokelaar, B.P.; Durant, G.P. The submarine eruption and erosion of Surtla (Surtsey), Iceland. *J. Volcanol. Geotherm. Res.* **1983**, *19*, 239–246. [CrossRef]
14. Rotolo, S.G.; Castorina, F.; Cellura, D.; Pompilio, M. Petrology and Geochemistry of Submarine Volcanism in the Sicily Channel Rift. *J. Geol.* **2006**, *114*, 355–365. [CrossRef] [PubMed]
15. Mazzarella, S. *Dell'isola Ferdinandea e di Altre Cose*; Sellerio Editore srl: Palermo, Italy, 2013.
16. Sinapi, L.; Lamberti, L.O.; Pizzeghello, N.M.; Ivaldi, R. The Graham Bank: Hydrographic features and safety of navigation. *Int. Hydrogr. Rev.* **2016**. Available online: https://journals.lib.unb.ca/index.php/ihr/article/view/25811 (accessed on 9 July 2026). [CrossRef]
17. Scarascia, S.; Cassinis, R.; Lozej, A.; Nebuloni, A. A seismic and gravimetric model of crustal structures across the Sicily Channel Rift Zone. *Boll. Della Soc. Geol. Ital.* **2000**, *119*, 213–222.
18. Agius, M.R.; Magrini, F.; Diaferia, G.; Kästle, E.D.; Cammarano, F.; Faccenna, C.; Funiciello, F.; van der Meijde, M. Shear-Velocity Structure and Dynamics Beneath the Sicily Channel and Surrounding Regions of the Central Mediterranean Inferred From Seismic Surface Waves. *Geochem. Geophys. Geosyst.* **2022**, *23*, e2022GC010394. [CrossRef]
19. Gaberšek, S.; Sorgente, R.; Natale, S.; Ribotti, A.; Olita, A.; Astraldi, M.; Borghini, M. The Sicily Channel Regional Model forecasting system: Initial boundary conditions sensitivity and case study evaluation. *Ocean Sci.* **2007**, *3*, 31–41. [CrossRef]
20. Lodolo, E.; Civile, D.; Zanolla, C.; Geletti, R. Magnetic signature of the Sicily Channel volcanism. *Mar. Geophys. Res.* **2012**, *33*, 33–44. [CrossRef]
21. Calò, M.; Parisi, L. Evidences of a lithospheric fault zone in the Sicily Channel continental rift (southern Italy) from instrumental seismicity data. *Geophys. J. Int.* **2014**, *199*, 219–225. [CrossRef]
22. Max, M.D.; Kristensen, A.; Michelozzi, E. Small scale Plio-Quaternary sequence stratigraphy and shallow geology of the west-central Malta Plateau. In *Geological Development of the Sicilian-Tunisian Platform*; UNESCO: Urbino, Italy, 1993; pp. 117–122.

23. Todaro, S.; Sulli, A.; Spatola, D.; Basilone, G.; Aronica, S. Seismic stratigraphy of the north-westernmost area of the Malta Plateau (Sicily Channel): The Middle Pleistocene-Holocene sedimentation in a tidally influenced shelf. *Mar. Geol.* **2022**, *445*, 106740. [CrossRef]
24. Todaro, S.; Sulli, A.; Spatola, D.; Micallef, A.; Di Stefano, P.; Basilone, G. Depositional mechanism of the upper Pliocene-Pleistocene shelf-slope system of the western Malta Plateau (Sicily Channel). *Sediment. Geol.* **2021**, *417*, 105882. [CrossRef]
25. Jongsma, D.; van Hinte, J.E.; Woodside, J.M. Geologic structure and neotectonics of the North African Continental Margin south of Sicily. *Mar. Pet. Geol.* **1985**, *2*, 156–179. [CrossRef]
26. Scandone, P. Mesozoic and Cenozoic rocks from the Malta Escarpment (central Mediterranean). *Am. Assoc. Pet. Geol. Bull.* **1981**, *65*, 1299–1319. [CrossRef]
27. Bosellini, A. Dinosaurs "re-write" the geodynamics of the eastern Mediterranean and the paleogeography of the Apulia Platform. *Earth-Sci. Rev.* **2002**, *59*, 211–234. [CrossRef]
28. Beccaluva, L.; Colantoni, P.; Savelli, C.; Di Girolamo, P. Upper-Miocene submarine volcanism in the Strait of Sicily (Banco senza Nome). *Bull. Volcanol.* **1981**, *44*, 573–581. [CrossRef]
29. Guidoboni, E.; Muggia, A.; Marconi, C.; Boschi, E. A case study in archaeoseismology. The collapses of the Selinunte temples (Southwestern Sicily): Two earthquakes identified. *Bull. Seismol. Soc. Am.* **2002**, *92*, 2961–2982. [CrossRef]
30. Parello, F.; Allard, P.; D'Alessandro, W.; Federico, C.; Jean-Baptiste, P.; Catani, O. Isotope geochemistry of Pantelleria volcanic fluids, Sicily Channel rift: A mantle volatile end-member for volcanism in southern Europe. *Earth Planet. Sci. Lett.* **2000**, *180*, 325–339. [CrossRef]
31. ViDEPI Project. *Visibility of Petroleum Exploration Data in Italy*; MISE: Rome, Italy; Ministero dello Sviluppo Economico DGRME: Rome, Italy; Società Geologica Italiana: Rome, Italy; Assomineraria: Rome, Italy, 2012.
32. Farrán, M. IMAGE2SEGY: Una aplicación informática para la conversión de imágenes de perfiles sísmicos a ficheros en formato SEG Y. *Geotemas* **2008**, *10*, 1215–1218. [CrossRef]
33. Grosse, P.; van Wyk de Vries, B.; Petrinovic, I.A.; Euillades, P.A.; Alvarado, G.E. Morphometry and evolution of arc volcanoes. *Geology* **2009**, *37*, 651–654. [CrossRef]
34. Basilone, L.; Spatola, D.; Sulli, A.; Basilone, G. Geomorphological characterization and marine geohazard assessment of mass transport deposits in the Graham Bank (Sicily Channel, Central Mediterranean). *Landslides* **2026**, *2026*, 1–18. [CrossRef]
35. Civile, D.; Lodolo, E.; Tortorici, L.; Lanzafame, G.; Brancolini, G. Relationships between magmatism and tectonics in a continental rift: The Pantelleria Island region (Sicily Channel, Italy). *Mar. Geol.* **2008**, *251*, 32–46. [CrossRef]
36. Ferranti, L.; Pepe, F.; Barreca, G.; Meccariello, M.; Monaco, C. Multi-temporal tectonic evolution of Capo Granitola and Sciacca foreland transcurrent faults (Sicily Channel). *Tectonophysics* **2019**, *765*, 187–204. [CrossRef]
37. White, J.D.L.; Houghton, B. Surtseyan and related phreatomagmatic eruptions. In *Encyclopedia of Volcanoes*; Academic Press: Cambridge, MA, USA, 2000; pp. 495–511.
38. Pedersen, G.; Grosse, P. Morphometry of subaerial shield volcanoes and glaciovolcanoes from Reykjanes Peninsula, Iceland: Effects of eruption environment. *J. Volcanol. Geotherm. Res.* **2014**, *282*, 115–133. [CrossRef]
39. Barreca, G. Gravimetric gradient, Sicily and southern Calabria, Italy (Central Mediterranean). *J. Maps* **2014**, *10*, 563–568. [CrossRef]
40. Hovland, M.; Gardner, J.V.; Judd, A.G. The significance of pockmarks to understanding fluid flow processes and geohazards. *Geofluids* **2002**, *2*, 127–136. [CrossRef]
41. Micallef, A.; Berndt, C.; Debono, G. Fluid flow systems of the Malta Plateau, Central Mediterranean Sea. *Mar. Geol.* **2011**, *284*, 74–85. [CrossRef]
42. Micallef, A.; Spatola, D.; Caracausi, A.; Italiano, F.; Barreca, G.; D'Amico, S.; Petronio, L.; Coren, F.; Facchin, L.; Blanos, R.; et al. Active degassing across the Maltese Islands (Mediterranean Sea) and implications for its neotectonics. *Mar. Pet. Geol.* **2019**, *104*, 361–374. [CrossRef]
43. Spatola, D.; Micallef, A.; Sulli, A.; Basilone, L.; Basilone, G. Evidence of active fluid seepage (AFS) in the southern region of the central Mediterranean Sea. *Measurement* **2018**, *128*, 247–253. [CrossRef]
44. Spatola, D.; Rovere, M.; Casalbore, D.; Chiocci, F.L. Pockmarks of the Mediterranean region seas: A comprehensive Geodatabase for Marine Geomorphological Analysis. *Sci. Data* **2025**, *12*, 1049. [CrossRef] [PubMed]
45. Lawal, M.A.; Cook, A.E. Gas migration phenomena and pockmark evolution in a Gulf of Mexico minibasin. *Mar. Pet. Geol.* **2025**, *173*, 107270. [CrossRef]
46. Stow, D.A.V.; Hunter, S.; Wilkinson, D.; Hernández-Molina, F.J. The nature of contourite deposition. *Dev. Sedimentol.* **2008**, *60*, 143–156. [CrossRef]
47. Viana, A.R.; Faugères, J.C.; Stow, D.A.V. Bottom-current-controlled sand deposits—A review of modern shallow- to deep-water environments. *Sediment. Geol.* **1998**, *115*, 53–80. [CrossRef]
48. Millot, C. Circulation in the Western Mediterranean Sea. *J. Mar. Syst.* **1999**, *20*, 423–442. [CrossRef]
49. Festa, A.; Dilek, Y.; Gawlick, H.-J.; Missoni, S. Mass-transport deposits, olistostromes and soft-sediment deformation in modern and ancient continental margins, and associated natural hazards. *Mar. Geol.* **2014**, *356*, 1–4. [CrossRef]

50. Dalla Valle, G.; Gamberi, F. Slope channel formation, evolution and backfilling in a wide shelf, passive continental margin (Northeastern Sardinia slope, Central Tyrrhenian Sea). *Mar. Geol.* **2011**, *286*, 95–105. [CrossRef]
51. Gamboa, D.; Alves, T.; Cartwright, J.; Terrinha, P. MTD distribution on a 'passive' continental margin: The Espírito Santo Basin (SE Brazil) during the Palaeogene. *Mar. Pet. Geol.* **2010**, *27*, 1311–1324. [CrossRef]
52. Urgeles, R.; Camerlenghi, A. Submarine landslides of the Mediterranean Sea: Trigger mechanisms, dynamics, and frequency-magnitude distribution. *J. Geophys. Res. Earth Surf.* **2013**, *118*, 2600–2618. [CrossRef]
53. Latter, J.H. Tsunamis of volcanic origin: Summary of causes, with particular reference to Krakatoa, 1883. *Bull. Volcanol.* **1981**, *44*, 467–490. [CrossRef]
54. Galea, P. Seismic history of the Maltese islands and considerations on seismic risk. *Ann. Geophys.* **2007**, *50*, 725–740. [CrossRef]
55. Hürlimann, M.; Ledesma, A.; Martí, J. Characterisation of a volcanic residual soil and its implications for large landslide phenomena: Application to Tenerife, Canary Islands. *Eng. Geol.* **2001**, *59*, 115–132. [CrossRef]
56. Ruiz, C.R.; García-Cacho, L.; Araña, V.; Luque, A.Y.; Felpeto, A. Submarine volcanism surrounding Tenerife, Canary Islands: Implications for tectonic controls, and oceanic shield forming processes. *J. Volcanol. Geotherm. Res.* **2000**, *103*, 105–119. [CrossRef]
57. Moore, J.G.; Jakobsson, S.; Holmjarn, J. Subsidence of Surtsey volcano, 1967–1991. *Bull. Volcanol.* **1992**, *55*, 17–24. [CrossRef]
58. Schmidt, R.; Schmincke, H.-U. Seamounts and Island Building. In *Encyclopedia of Volcanoes*; Academic Press: Cambridge, MA, USA, 1999; pp. 383–402.
59. Romagnoli, C.; Jakobsson, S.P. Post-eruptive morphological evolution of island volcanoes: Surtsey as a modern case study. *Geomorphology* **2015**, *250*, 384–396. [CrossRef]
60. Clark, P.U.; Dyke, A.S.; Shakun, J.D.; Carlson, A.E.; Clark, J.; Wohlfarth, B.; Mitrovica, J.X.; Hostetler, S.W.; McCabe, A.M. The last glacial maximum. *Science* **2009**, *325*, 710–714. [CrossRef] [PubMed]
61. Ramalho, R.S.; Quartau, R.; Trenhaile, A.S.; Mitchell, N.C.; Woodroffe, C.D.; Ávila, S.P. Coastal evolution on volcanic oceanic islands: A complex interplay between volcanism, erosion, sedimentation, sea-level change and biogenic production. *Earth-Sci. Rev.* **2013**, *127*, 140–170. [CrossRef]
62. Civile, D.; Lodolo, E.; Accettella, D.; Geletti, R.; Ben-Avraham, Z.; Deponte, M.; Facchin, L.; Ramella, R.; Romeo, R. The Pantelleria graben (Sicily Channel, Central Mediterranean): An example of intraplate "passive" rift. *Tectonophysics* **2010**, *490*, 173–183. [CrossRef]
63. Quinci, E.M.; Torri, M.; Cuttitta, A.; Patti, B. Predicting potential spawning habitat by ensemble species distribution models: The case study of European anchovy (Engraulis encrasicolus) in the strait of Sicily. *Water* **2022**, *14*, 1400. [CrossRef]
64. Bouramdane, A.-A. Natural Gas Transit from West Africa to Europe (Africa Atlantic Gas Pipeline) to Maximize Energy Security and Transit Revenues by 2050. *J. Geo-Energy Environ.* **2026**, *2*, 1–33. [CrossRef]
65. Benaïchouche, S.; Le Goff, C.; Boussidi, B.; Rousseau, F.; Fablet, R. Learnable variational models for the reconstruction of sea surface currents using ais data streams: A case study on the sicily channel. In Proceedings of the IGARSS 2022-2022 IEEE International Geoscience and Remote Sensing Symposium, Kuala Lumpur, Malaysia, 17–22 July 2022; pp. 6821–6824.

Disclaimer/Publisher's Note: The statements, opinions and data contained in all publications are solely those of the individual author(s) and contributor(s) and not of MDPI and/or the editor(s). MDPI and/or the editor(s) disclaim responsibility for any injury to people or property resulting from any ideas, methods, instructions or products referred to in the content.